Electronic, Structural, and Magnetic Upgrading of Coal-Based Products through Laser Annealing

Xining Zang,* Nicola Ferralis, and Jeffrey C. Grossman

Cite This: https://doi.org/10.1021/acsnano.1c07693

Read Online

ACCESS | Metrics & More | Article Recommendations | Supporting Information

ABSTRACT: Most coal-to-product routes require complex thermal treatment to carbonize the raw materials. However, the lack of unified comparison of products made from different kinds of coals downplays the role of initial coal chemistry in high-temperature reactions. Here, we used a CO_2 laser to investigate the roles that aromatic content and maturity play in the structural evolution and doping of coals during annealing. Results show that a bituminous coal (DECS 19) with aromatic content and maturity in between higher rank, more mature anthracite (DECS 21) and lower rank, lower maturity lignite (DECS 25) leads to more graphite-like structure observed from the highest 2D peak on the Raman spectrum and conductivity (sheet resistance ~30 ohm sq^{-1}) after lasing. When nitrogen dopants are incorporated with saturated urea dopants into coals through laser ablation, nitrogen preferentially incorporates at the edge sites of graphitic grains. Furthermore, oxide nanoparticles can be incorporated into the graphitic backbone of coal to modify their electronic and magnetic properties through laser annealing. Leveraging tunable magnetic behavior, we demonstrate a soft actuator using both conductive and magnetic coal-Fe/Co oxide. Through laser annealing, we propose a paradigm to understand and control coal chemistry toward flexible and tunable doping and magnetism.
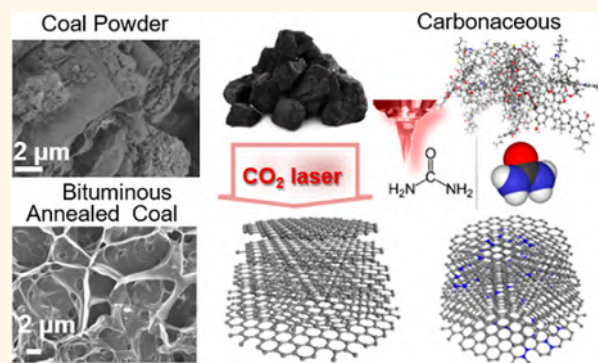
KEYWORDS: coal, laser annealing, doping, polyaromatic hydrocarbons, thin film electronics

INTRODUCTION

Current state-of-the-art coal-to-products primarily consists of coal-derived feedstocks (including rare earths),[1,2] carbon fibers from coal tar pitch,[3−6] carbon black for rubber tires,[7] coal-derived graphite,[8] and active carbon, among other uses. The synthesis of carbon materials from coal has received renewed interest due to the extensive, broad, and cheap availability of coal as a feedstock.[9,10] Through advanced chemistry and materials processing, coal-derived functional materials have been developed including graphene oxide,[11] carbon quantum dots,[12] and carbon nanotubes,[13] which have been applied in photovoltaics,[14] energy storage devices,[15] and sensors (Table S1).[16,17] Beyond coal-derived materials, the thin film electronics that can be manufactured in a continuous (i.e., roll-to-roll) method are desired for scalable applications of coal feedstocks.[18] Therefore, a deeper understanding and nanoscale control of coal graphitization, including manipulation of electronic, magnetic, and structural properties, will amplify the potential of these nontraditional routes of coal commercialization by enabling the design and ordering of functional units at the molecular level.

In this work, we select coals with three rankings (Table S2),[19] to investigate the role of coal chemistry, rank in determining the quality of graphitization, and dopant and metallic incorporation using a CO_2 laser as a local heating source.[20] The three coals selected are anthracite (DECS 21), low-volatile bituminous (lvB, DECS 19), and lignite (DECS 25), with decreasing rank, aromatic content, and vitrinite reflectance (VR$_o$),[19,21] which is a measure of maturity. Detailed properties of these three typical coals are listed in Table S2. The coal molecular structures can be illustrated as aromatic−hydroaromatic clusters connected by aliphatic (alkanes) and ether bridges. Anthracites have large aromatic clusters and low content of alkane bridges; lignite coals are primarily composed
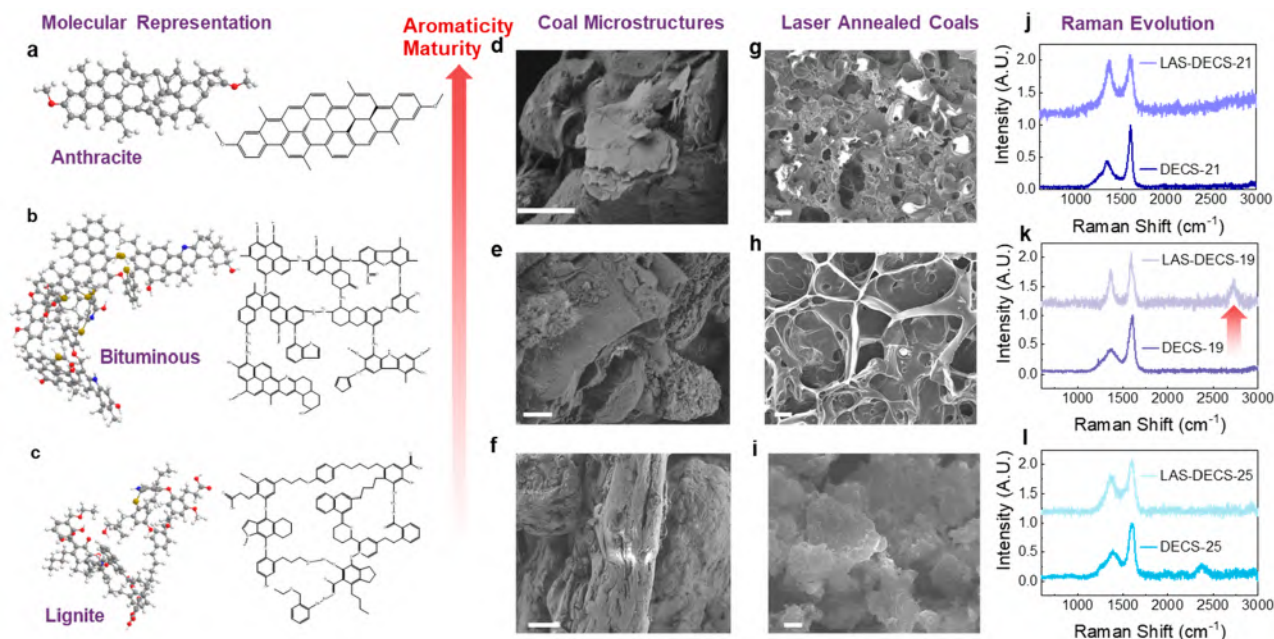
Figure 1. Dependence of maturity on the microstructure of coals upon laser annealing. (a−c) Typical molecular representations of anthracite, bituminous, and lignite coals.[29] (d−f) Scanning electron microscopic (SEM) images of DECS 21 (anthracite coal), DECS 19 (low-volatile bituminous coal), and DECS 25 (lignite coal). (g−i) SEM images of laser-annealed coals in (d)−(f). Scale bars in (d)−(i): 2 μm. (j−l) Raman spectra of different coals before (d−f) and after laser annealing (g−i).

of phenols interconnected by an alkane of different lengths (from C1 to C5); and bituminous coals lie in between with both rich aromatic backbones and alkane bridges. A typical molecular representation of each coal is illustrated in Figure 1a−c. The higher VR_o refers to the higher condensation of aromatic structures, $i.e.$, larger aromatic clusters and higher aromatic content, in the coal matrix.[22,23]

Previously, Lin et al.[12,24] and Ye et al.[25] have successfully derived porous graphene materials from coal and wood using a laser as a heat source. We extend the investigation of laser annealing of coal to reveal how the initial coal chemistry affects the electronic properties of laser-processed carbon materials, with the aim of developing consistent fabrication routes leading to carbon films with well-defined electronic properties. Furthermore, we explore how the final properties can be further improved by the tunability of their electronic and magnetic behavior through doping. Coal thin films are deposited using coal suspensions with and without urea as a dopant. As-deposited films are carbonized and graphitized at high temperature in air via laser ablation.[16,26,27] The results show that DECS 19 with intermediate VR_o (1.71%) and aromatic content shows the highest amount of graphitic structure after laser annealing, while the most mature DECS 21 (VR_o 5.19%) and least mature lignite coal DECS 25 (VR_o 0.23%) show rare graphitization reflected by the absence of a 2D Raman peak.[28] Sheet resistances of the laser-annealed coals increase following the descending order of coal graphitization, and the lowest sheet resistance of lased bituminous (DECS 19) is ∼30 ohm sq^{-1}.

Meanwhile, laser doping using urea as a dopant source shows a decreasing trend of incorporation efficiencies with the increase of graphitic content of coals. The N substitution shows a preference for edge positions. Nitrogen substitutions in graphitic positions appear in lased, doped DECS 21 and DECS 19, indicating a necessity of graphitic condensation for

graphitic-N incorporation. Leveraging the role of nanostructure (defects, edges, sheet size, and distribution) in defining the incorporation of heteroatoms, using laser annealing we decorate metallic nanostructures onto coal's aromatic cores, to make active electronic devices such as soft actuators from conductive and magnetic coal-Fe/Co oxide.

RESULTS AND DISCUSSION

Laser Annealing of Coals. Figure 1a, b, and c are representative molecular fragments of these coals at room temperature. In coals the molecular structure is not as well defined as it would be in crystals or polymers, but rather as a comprehensive distribution of small molecular structures that can be largely characterized with mass spectrometry, NMR, elemental analysis, and vibrational spectroscopy. In developing visual models for such systems, a statistical approach is usually adopted, where the most representative molecular sets are often considered for visualization.[30−32] Filtered coal particles (<2 μm) derived from supernatants from each type of coal are dispersed in distilled water (5 mg mL^{-1}) and deposited via drop-casting onto glass to make coal thin films.[18] We used a CO$_2$ laser (10.6 μm) to anneal each coal thin film (deposition and laser processing details can be found in the Supporting Information). Laser-annealed thin films show different morphologies and structures depending on their original chemistry (Figure 1). As shown in SEM micrographs, the nonuniform discrete coal thin films of DECS 21 and 19 (Figure 1d,e) are merged into continuous porous structures upon lasing (Figure 1g,h), indicating a reconstruction of the heavy hydrocarbons. In contrast, ablated lignite exhibits a disrupted cluster-like structure, with no homogeneous pore distribution, unlike the others, although larger coal particles break into smaller percolated coal particles (Figure 1f and i).

The release of volatile organic compounds (VOCs), dehydrogenation at aromatic edges, and decomposing of
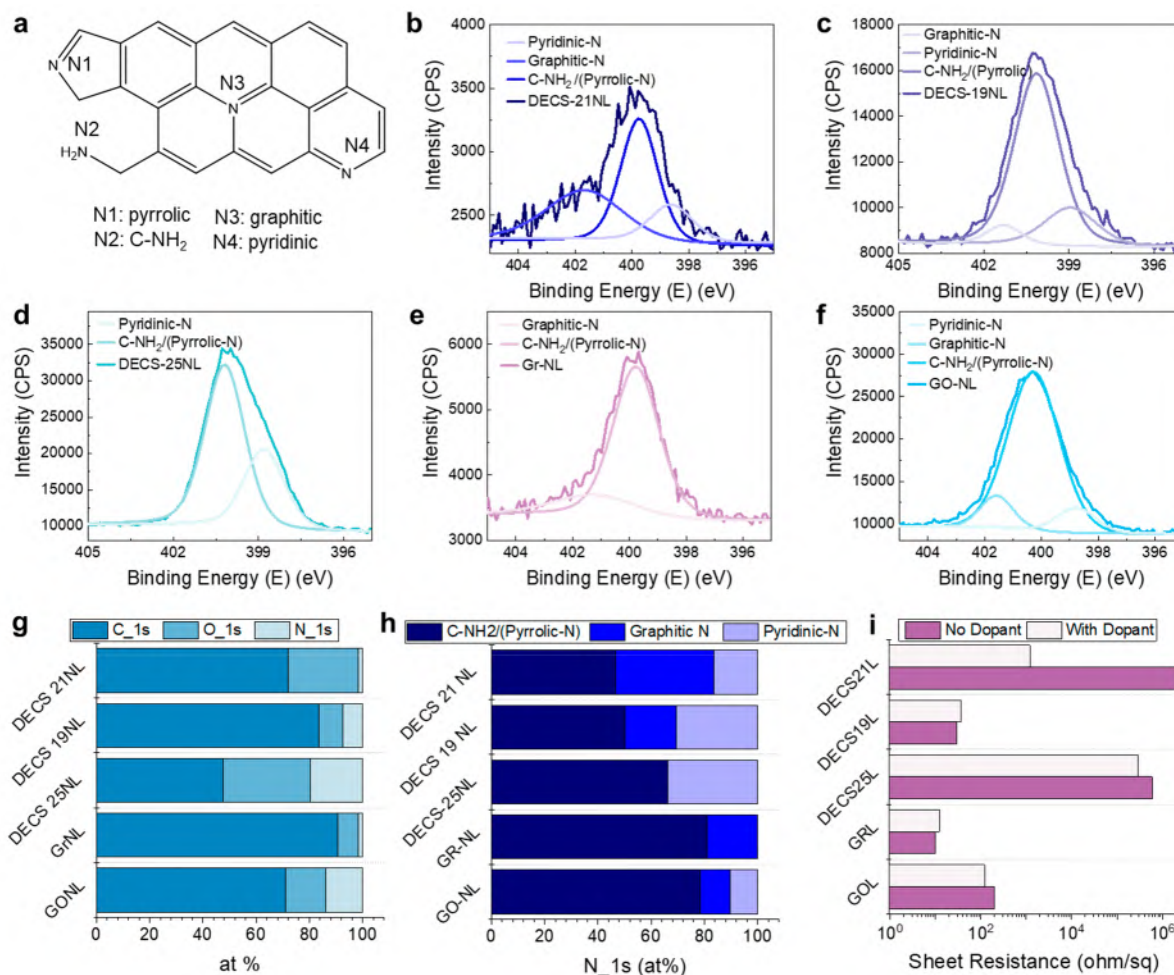
Figure 2. Effects of laser annealing on nitrogen doping from maturity and microstructure of coals. (a) Schematics of different N dopant positions. (b−f) X-ray photoelectron spectroscopy (XPS) spectra of N_1s peaks of different coals, graphene pellet (GR), and graphene oxide (GO). (g) C, O, N component atomic ratios of laser-doped coals, GR, and GO. (h) Pyrrolic, graphitic, and pyridinic nitrogen ratio of (a)−(f). (i) Sheet resistance of laser-annealed and -doped coals, GR, and GO.

VOCs introduce pore structures, which increase in size with volatile matter ratio (Figure S1, Figure 1g,h). The high concentration of alkanes in lignite and relatively small aromatics, often phenols,[33] leads to a significant release of VOCs through fast pyrolysis during lasing at up to >2000 °C.[16,20,34] On the contrary, the large aromatic backbone in anthracite provides greater stability, such that only small VOCs are released upon lasing and the remaining structure fuses. Bituminous is in the middle, where more disruption is expected through VOC release but can enable aromatic sheets to better align and stack. As shown in Figure S1, laser-annealed high-volatile bituminous (hvB) coal shows more visible pores than laser-annealed low-lvB coal due to the higher content of VOCs. In mild and slow furnace annealing, the carbonaceous networks reorganize during the annealing, with less dramatic release of VOCs and thus smaller and fewer pores compared to laser annealing.[18]

Laser-annealed bituminous (DECS 19) presents 2D peaks near 2750 cm^{-1} in their Raman spectra, indicating graphitic stacking (Figure 1k), while laser-processed anthracite (DECS 21) and lignite (DECS 25) thin films do not show 2D peaks (Figure 1j and l). From the Raman spectra shown in Figure 1j−l, we notice that the full width at half-maximum (fwhm) values of the D peaks (~1350 cm^{-1}) on the Raman spectra of

bituminous, anthracite, and lignite decreased by 23.7%, 72.7%, and 34.2%, respectively, relative to that of unannealed samples. The narrowing of the D peak indicates a decrease in sp^2 disorder during annealing or increase in the size of aromatic cores (Figure S2a).[35] The fwhm of the G peak (~1600 cm^{-1}) in the Raman spectrum of laser-annealed bituminous (DECS 19) decreases by 24.2% (Figure S2b), indicating the formation of larger graphitic clusters.[28] Furthermore, the G peak of laser-annealed anthracite (DECS 21) broadens compared to the nonablated DECS 21, indicating a potential reduction in the aromatic size. These results are consistent with previous investigations of laser annealing of heavy hydrocarbons, where it was shown that native extended aromatic sheets require aliphatic functional groups as a carbon source during the annealing process in order to form larger graphitic clusters upon lasing.[16,36] Previously, we also found that adding small aromatic molecules, such as hexamethylbenzene (hMB), can further improve the graphitic structures and their stacking upon lasing with octane.[16] The stabilization of graphitic structures by hMB additive molecules can explain the most effective graphitization in laser-annealed lvB coal (DECS 19) with distributed size of aromatics and aliphatics (alkanes).[16] In Figure S3, the I_{2D}/I_G ratio on the Raman spectrum of laser-annealed high-volatile bituminous coal (LAS-DECS-31) rises
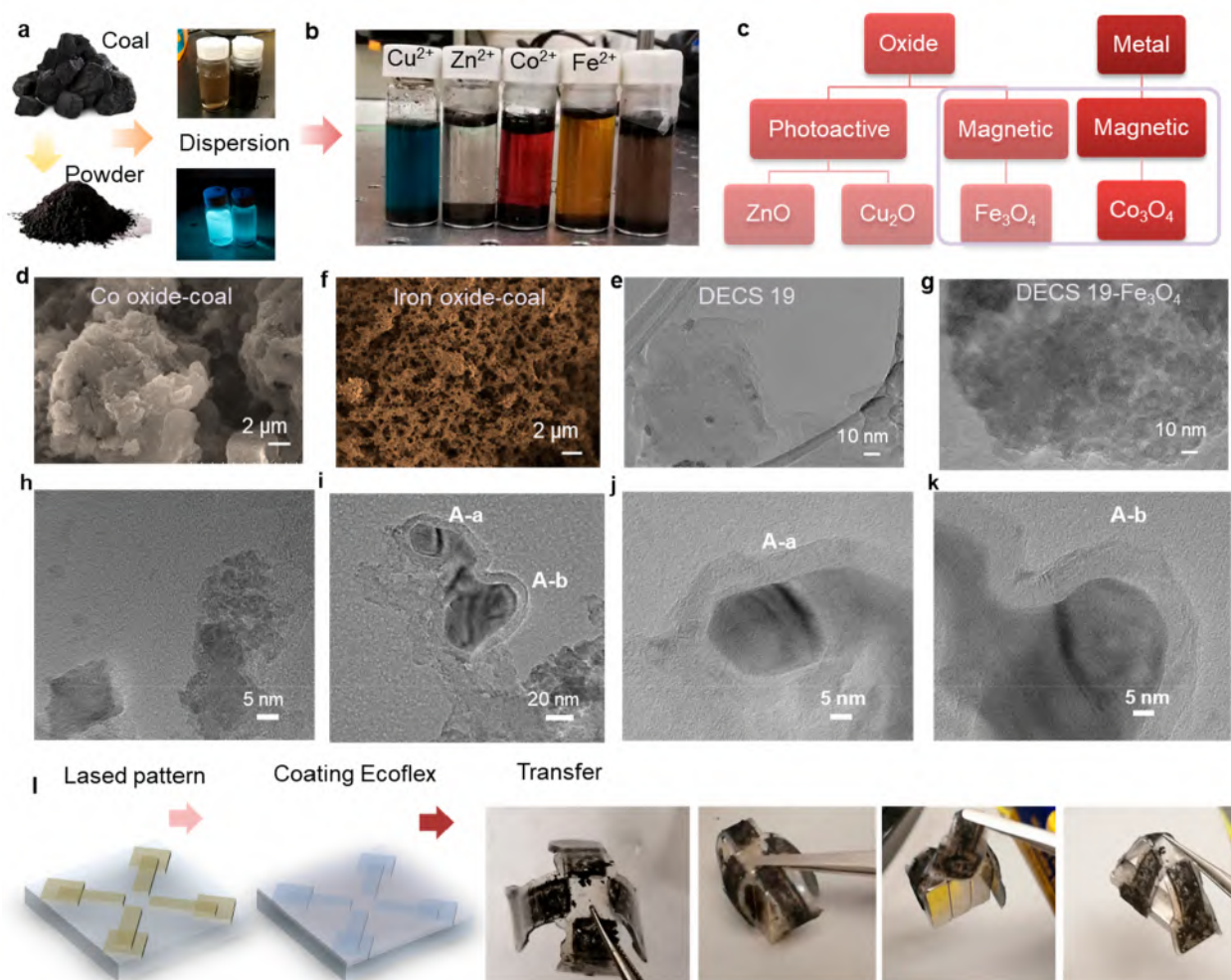
C

Figure 3. Integration of functional structure onto coals and application in magnetic devices. (a) Schematic of making coal powder suspensions. (b) Soaking coal powders in solutions with different metal ions. (c) Functional materials that can be incorporated into coals using laser processing. (d) SEM images of coal decorated with Co_3O_4 particles from the coal-$CoCl_2$ precursor. (e) SEM images of coal decorated with Fe_3O_4 particles from the coal-$FeCl_3$ precursor. (f) Transmission electron microscopy (TEM) image of DECS 19 coal dispersed onto a copper grid. (g) TEM image of coal-Fe_3O_4 dispersed onto a copper grid. (h−k) Transmission electron microscopic (TEM) image of graphitic carbon layers grown on the iron oxide nanoparticle surfaces. (j) and (k) are zoomed-in TEM images of selected areas in (i), showing around 5 nm thick graphite layers stacking conformally on the nanoparticles. (l) Schematic of using a laser to pattern a coal-Fe_3O_4 flexible device. Optical images of an Ecoflex transferred coal-Fe_3O_4 gripper to lift a magnet with >10 times heavier weight.

to 0.56, while that of the raw DECS 31 is near zero. The I_{2D}/I_G ratio of LAS-DECS-31 at 0.56 is close to that of laser-annealed low-volatile bituminous coal (LAS-DECS-19) at 0.53, indicating similar graphitization degrees. Such results support the previous findings that close chemistries (VR$_o$, H:C ratio, *etc.*) lead to similar graphitic structures (Table S1), in the coexistence of aromatics and aliphatics.

Doping of Coals *via* Laser Annealing. Doping graphitic carbon materials has long been used as a means to modify their band structure,[37,38] improve conductivities,[33,39] and introduce a host of other properties, such as in the case of ferromagnetism in N-doped graphene.[40] Physisorbed urea on coal is used as a dopant to incorporate nitrogen into the coal nanostructures, through laser annealing coal thin films. The C, H, and O atomic ratios of laser-annealed urea-doped thin films of anthracite, bituminous, and lignite are compared with laser-treated graphene pellets (Gr)-urea and graphene oxide (GO)-urea thin films, using X-ray photoelectron spectroscopy (XPS) measurements (Figure 2). The N_1s

peaks are composed of three subpeaks, where N_1s at 401.1, 400, and 398.3 eV represents the graphitic-N, pyridinic-N and free C-NH$_2$, and the pyrrolic-N,[41] respectively (Figure 2a). As a naming convention in the present work, N followed by the sample name refers to urea-doped samples, L refers to laser processing, and NL is used to denote laser doping using urea dopants. The deconvolution of the N_1s peaks of laser-doped coals, Gr, and GO is shown in Figure 2b−f. The efficiencies of laser incorporation of N into different laser-annealed coals follow a similar trend to the efficiencies to graphitize the same coals.

As shown in Figure 2g,h, N-incorporation in laser-doped DECS 19 NL (7.55 at. %) is significantly higher than for DECS 21 NL (1.51 at. %). Laser-ablated urea-doped DECS 25 (noted as DECS 25 NL) shows the nitrogen (19.8 at. %) content, since the lignite with rich aliphatic content and poor aromatic condensation could potentially offer more active sites for N incorporation. The majority of nitrogen doping groups are pyridinic (C-NH$_2$ type, N_1s) and pyrrolic N_1s on the edges

of the aromatic sheets, due to the reported lower energy barriers.[42,43]

Graphitic-N dopants only occur in laser-doped Gr, GO, DECS 21, and DECS 19 with higher maturity and aromatic content (Figure 2b−f,g,h). Previous experimental work in the work by Lin et al. shows that single pyridinic-N and graphitic (substitutional)-N increase the conductivity of intrinsic graphene from 7.29×10^3 S cm^{-1} to 9.30×10^3 S cm^{-1} and 1.96×10^4 S cm^{-1}, respectively, but decrease the carrier mobility by almost 1 order of magnitude in both cases.[41] Clustered graphitic-N (1.4 at. %) can promote the conductivity to 1.62×10^5 S cm^{-1} while retaining 80% of the carrier mobility. Graphitic-N is expected for more conductive aromatic structures.

Regarding electrical conductivity upon doping, we find that doped DECS 19 shows a sheet resistance of 36.4 ohm sq^{-1} (Figure 2i), which can be attributed to aligned ordering and broadly interconnected sheets reflected by the smaller fhwm's of the D peak and G peak, indicating lower disorder and larger aromatic cores (Figure S2). As also can been seen in Figure 2h,i, the significant number of graphitic-N dopants (∼40 at. %) helps to decrease the sheet resistance of laser-annealed DECS 21 from 2 M ohm sq^{-1} to 1200 ohm sq^{-1} in laser-doped DECS 21 NL. Due to the lack of effective graphitization, the laser-annealed DECS 25 shows high sheet resistance at 600 kohm sq^{-1}, while the dopants of nitrogen in highly oxidized DECS 25NL lower the resistance to 285 kohm sq^{-1}, possibly due to the formation of anchors and bridges that connect the carbonaceous network and provide additional electron pathways.[44]

We test these hypotheses to develop strategies to maximize charge transfer (doping) and increase interconnectivity by using Gr and GO as comparisons and perform laser ablation with an aliphatic carbon source (octane, noted as O) and nitrogen source (urea, noted as N) in Figure S4, where L refers to laser ablation. As shown in Figure 2e and Figures S4 and S5, the lased Gr (GrL) thin film results in almost identical XPS and Raman spectra compared to that of the as-deposited Gr thin film, which is expected due to the minimal changes in distribution of already large graphitic sheets. Upon deposition of physisorbed urea, nitrogen levels in GrN (1.58 at. %) decrease to 1.19 at. % in GrNL after annealing, and of this, 19 at. % is graphitic-N (Figure 2e,h), indicating N-incorporation into the graphitic lattice. Laser-processed Gr with both a nitrogen source and octane (GrONL) shows the highest incorporation of nitrogen at 2.03 at. %. We note that laser-processed Gr thin films, with either octane, urea, or both, all show a significant decrease of the D peak in the Raman spectrum (Figure S3) and an increase of the I_G/I_D ratio, indicating the decrease of defects in the graphitic sheets. The healing of defects can be attributed to the filling of vacancies by the carbon atoms from octane.

As shown in Figure S4, laser annealing of GO thin films induces graphitic stacking, as indicated by the increased 2D peak,[35] while adding either octane or urea can promote the reduction of GO, and they consequently display a 2D peak as a result of reduction. Urea has been reported as an expansion−reduction agent of graphene oxide, owing to the reducing gas generated upon heating that can remove surface oxygen groups.[45,46] Octane functions similarly to urea as a reducing agent, while its additional carbon source helps to increase the graphitic structure forming during the laser processing of heavy hydrocarbons, which has also been reported in previous

work.[16] Lased GO thin films doped with urea show a significant reduction of O_1s content to 14.96 at. % from the 38.5 at. % in the as-deposited GO thin film, and 34% of the incorporated N dopants occupy the graphitic positions (Figure 2f−h).

Functionalization of Conductive Coal Thin Films. Besides tuning the electronic properties of coals by laser annealing and thermal doping, we investigate the possibility to integrate functional nanostructures on coals. In particular, we focus on lased and laser-doped thin films from select LvB coal (DECS 19) due to its (1) high electrical conductivity; (2) homogeneity within the thin film structure with relatively low porosity due to the low content of volatile matter;[22] and (3) feasibility as a platform to introduce dopants due to its intermediate aromatic structure with connecting aliphatics. As shown in Figure 3a, DECS 19 coal powders derived from the supernatant are dispersed in DI water. Different water-soluble metal salts are dissolved in the coal dispersions to make solutions with a concentration of ∼0.1 mol L^{-1} as shown in Figure 3b. Photoluminescence in Figure 3a indicates that the coal particles are dispersed uniformly in water, while the dissolved ions change the charge balance and cause coalescence of coal particles. Coal particles absorb the laser energy, without which laser annealing can hardly convert the metal ion salts into oxide particles. From the X-ray diffraction (XRD) results (Figure S6), we observe that coal-Cu, coal-Zn, coal-Co, and coal-Fe can be converted to conductive carbon with Cu_2O, ZnO, Co_3O_4, and Fe_3O_4 nano/microparticles (Figure 3c, Figure S6). Cu_2O and ZnO are known semiconductors that have been widely applied in photovoltaic applications,[47] and Co_3O_4 and Fe_3O_4 are magnetic materials that could be applied in electromagnetic devices including sensors, actuators, or waste treatment membranes, to name only a few examples.[48,49] This example shows how coal can be made conductive with controllably tuned electronic and magnetic properties through simple processing techniques.

We focus on the Co/Fe structures that can be integrated in coal to achieve a highly controllable magnetic behavior and without loss of the electrical and mechanical properties of the coal-based laser-annealed films. Using coal in a magnetic actuator serves three purposes: (1) acting as a binding agent for the magnetic particles, allowing fabrication of actuators of complex morphologies through simple fabrication methods; the hydrocarbons in coal particles absorb the laser energy, without which laser annealing can hardly convert the metal ion salts into oxide particles;[17] (2) allowing the integration of the fabrication of actuators with other coal-based devices within the same manufacturing stream; (3) tuning the electrical and magnetic properties at the same time, which may enable the development of an integrated sensing and actuating platform. We optimized the laser parameters to minimize the sheet resistance of coal-Co_3O_4 and coal-Fe_3O_4 thin films down to 52.1 and 78.1 ohm sq^{-1}, using parameters of (2.7 W, 6.3 mm s^{-1}) and (1.5 W, 4.9 mm s^{-1}), respectively (Figure S7). SEM images of laser-annealed Co_3O_4 and Fe_3O_4 particles on coal structures are shown in Figure 3d,e, and their magnetic characterization results are shown in Figure S8. Lased coal-Fe_3O_4 thin films show a more uniform porous morphology, compared to the clustered rough morphology of coal-Co_3O_4 thin films. From the transmission electron microscopy (TEM) image of DECS 19 coal and the laser-induced coal-Fe_3O_4, we observe that Fe_3O_4 particles with sizes of ∼10 nm are distributed uniformly onto the flakes of the original DECS 19

structure. We also noted that ~5 nm thick graphite layers form conformally on the nanoparticles, as shown in the zoomed-in TEM images in Figure 3h–k.

Laser-annealed coal-Fe_3O_4 shows higher saturation magnetization (M_s) at 49.2 emu g^{-1} than that of coal-Co_3O_4 (18.1 emu g^{-1}) and higher remanence (Br) at 9.8 emu g^{-1} than that of coal-Co_3O_4 (3.2 emu g^{-1}). The coal-Fe_3O_4 shows similar ferromagnetic behavior compared to Fe_3O_4.[48,50] A prototype coal-Fe_3O_4-based flexible magnetic actuator is shown in Figure 3l, where a coal-Fe_3O_4-based actuator transferred onto Ecoflex with 0.9 g weight can lift a magnet (NdFeB) over 10 times heavier. The laser annealing in this work provides a technique to tune, simultaneously, yet with independent control the magnetic behavior of coal from electrical conductivity. The unified method to control the electromagnetic properties of coals can broaden their applications in more areas including soft electromagnetic actuators,[51] radio frequency (RF) micro-electromechanical systems (MEMS),[52] and more. Using coal as a single feedstock combined with laser annealing, we can potentially print sensors and actuators, transmitters, and receivers by the same manufacturing flow.

CONCLUSION

In this paper, we systematically investigate the effects of the initial chemical makeup of coal in the graphitization of polycyclic aromatic hydrocarbons, in the presence of nitrogen dopant or metallic particles under annealing at high temperature using a CO_2 laser. Leveraging the work done by Nature in customizing the chemistry and structure of coals, a single laser process can be used to control the graphitic content, porous morphology, dopant position, and electronic properties of processed products.

We find that (1) highly aromatic structures (Gr and DECS 21) do not form significantly larger graphitic structures under high-temperature annealing than those natively present nor can dopants be effectively incorporated; (2) aliphatic content provides carbon that can be mobilized during annealing to form conjugated interconnections among aromatic sheets into extended graphitic clusters and to incorporate the dopant into graphitic sheets; (3) for all coals most of the nitrogen dopants occupy the edge positions (pyrrolic, C-NH_2, and pyridinic N); and (4) graphitic-N substitution can be triggered by laser-induced high temperature onto a highly graphitic structure (Gr, GO, DECS 21, DECS 19), which contributes most to increase the conductivity of as-lased coal aromatic structures. As such, bituminous coals have more potential to graphitize compared to anthracite coals with rich aromatic and lignite coals with rich aliphatic content,[53] which also function as a better backbone to hold graphitic-N dopants upon lasing.

Furthermore, we also developed a versatile method to integrate other functional groups such as oxides and metal nanoparticles within the coal structure, using solution coating and laser annealing, which can potentially be adapted for use in large-scale manufacturing. We use such methods to fabricate a soft magnetic gripper based on bituminous coal decorated with Fe_3O_4. The understanding of coal hydrocarbon evolution induced by laser annealing provides the guidance to control and modify the coal structural and electronic properties for precise applications that might require strict control over porosity and electronic and magnetic behavior. The flexibility of coal as a feedstock holds promise that a similar approach may be also applicable to other heavy hydrocarbons such as tar, pitch, and asphaltene.

EXPERIMENTAL SECTION/METHODS

Materials. Coal samples were provided by the Penn State Coal bank,[54] and the as-received coal powder samples were ground below 60 μm in size. Graphene pellets were from XG Sciences, xGnP-C-300. The graphene oxide suspension (2 mg mL^{-1}) was purchased from Sigma-Aldrich. Urea (≥98 wt %) powder was purchased from Sigma-Aldrich. $CoCl_2$ (≥97 wt %), $Cu(NO_3)_2$ (≥97 wt %), $ZnCl_2$ (≥98 wt %), and $FeCl_3$ (≥97 wt %) came from Sigma-Aldrich.

Methods. *Materials Characterization.* A profilometer (Bruker DXT Stylus profilometer) was used to map the thickness of spin-coated and laser-ablated thin films. Scanning electron microscopy (SEM, Hitachi SU8100) and transmission electron microscopy (JEOL 2011 high-contrast TEM) were employed to study the morphology and structure. X-ray photoelectron spectroscopy (Thermo Scientific K-Alpha XPS) was used to study the surface element components of samples. An Al k-alpha microfocused monochromator with variable spot size (30−400 μm in 5 μm steps) was used. Micro-Raman spectra were acquired using a Renishaw inVia confocal Raman microscope using a 473 nm excitation source. The laser spot on the sample was ~800 nm in diameter and had a power of ~4 mW at the sample surface. The full spectral window for each acquisition was from 600 to 3200 cm^{-1}. Sheet resistance was tested by a four-point probe. X-ray powder diffraction was performed using a Panalytical multipurpose diffractometer. Semiquantitative analysis of patterns was performed using HighScore software to identify the phases and estimate the components.

Magnetization Measurement of Coal Composites. Magnetism measurements of coal composite samples were performed using the magnetic property measurement system equipped with a vibrating sample magnetometer from Quantum Design, USA. Hysteresis loops were measured under static external magnetic fields ranging from −2400 to +2400 kOe. Magnetization values were corrected assuming the response of the sample holder, sample capsule, and respective Pascal constants.

Coal Suspensions and Thin Film Deposition. As received coal powders were dispersed in distilled (DI) water to precipitate the large particles, and the supernatants of different coals were filtered by polystyrene (PS) membranes (47 mm diameter, 2 μm pore size). Coals on membranes were dried in air and scratched off. Coal suspensions were dispersed in DI water again, sonicated for 1 h, and stirred for 24 h at 80 °C. Redispersed coal suspensions (5 mg mL^{-1}) were spin coated onto glass at 500 rpm min^{-1} and dried at 80 °C for 3 h to make a thin film.

Coal-Urea Thin Film Deposition. Coal powders selected by the supernatant DECS 21, 19, 31, and 25 were redispersed in DI water, adding 100 mg of urea to the coal suspension (5 mg mL^{-1}). The coal-urea suspension was stirred and heated for 24 h at 60 °C. The suspension was vacuum filtrated using PS membranes (47 mm diameter, 2 μm pore size) and washed with DI water three times. The washed coal on the PS membranes were dried at room temperature for 24 h, and the coal-powder with absorbed urea was scratched off and redispersed in DI water with high concentration (20 mg mL^{-1}). Such suspensions were spin coated onto glass at 500 rpm/min and dried at 80 °C for 3 h to make a thin film.

Doped/Undoped Graphene Pellet and Graphene Oxide Thin Films. Thin films of graphene pellets and Gr-urea were deposited using the same process as for the coals. We directly spin-coated a graphene oxide suspension onto glass slides at 100 rpm/min and let the thin film dry in air for 48 h. To make the GO-urea thin film, 10 mg of urea was added into 20 mL of a 4 mg/mL graphene oxide suspension, which was stirred for 24 h. The GO-urea suspension was also spin-coated onto glass slides and dried in air. We did not heat to hasten the drying process since GO could be reduced by urea at elevated temperature.[55]

Doped/Undoped Graphene Pellet and Graphene Oxide Thin Films with Octane. Thin films of Gr and GO with and without dopant were deposited onto glass slides. A 10 μL amount of octane was dropped onto the samples with a size of 1 × 1 cm^2, and the samples were dried in air for 1 h before laser annealing.

Laser Annealing and Laser Doping of Coals, Gr, and GO. A commercial Universal VSL 2.30 laser cutter was utilized to perform the laser annealing in air, with a CO_2 laser tube (maximum power of 30 W) and all built-in optics. The laser spot was focused on the top surface of spin-coated films, and the height of the sample was controlled by tuning the *z*-position of the supporting cutting table. The designed device pattern was imported to a vector graphics software (Inkscape) and engraved by communicating with the laser cutter as a printer. On different coal films, different parameters of power and speed were crossed compared for maximum conductivity at the focus. We fixed the ablation speed at 10% (127 mm s^{-1}) and changed the power from 10% to 20% (3 W to 6 W). For different coal thin films, the highest conductivity was processed at various power, and the material characterizations reported in the paper were all on the samples with best conductivity and lowest sheet resistance. All the laser-annealed samples were heated to 300 °C to remove free urea, octane, and other volatile matter.

Decorating Coal with Other Functional Materials by Laser. DECS 19 coal powders with a smaller sized derived from the supernatant were dispersed in DI water. Different water-soluble salts ($CoCl_2$, $Cu(NO_3)_2$, $ZnCl_2$, and $FeCl_3$) were dissolved in the coal dispersions (10 g L^{-1}) to make solutions with a concentration of ~0.1 mol L^{-1}. The suspensions were subjected to ultrasound for 2 min before spin-coating onto slides. Laser annealed coal-metal salts were scratched off from the slides, washed, and separated by vacuum filtration for future characterizations.

Prototyping a Magnetic Coal-Based Soft Actuator. Coal-metal salt ($FeCl_3$) dispersions were spin-coated onto glass slides, and a computer-aided design software interface was employed to control the CO_2 laser to pattern the designed feature with optimized laser parameters. After laser patterning, the sample was washed with DI water to remove the nonablated coal and the residual salt, and then the patterned samples were dried in air for 24 h. Ecoflex (Ecoflex00-35) was poured onto the coal-Fe_3O_4 pattern at an amount of 1 mL cm^{-2} and cured for 5 min, after which we peeled off the sample from the glass surface.

ASSOCIATED CONTENT

Ⓢ Supporting Information

The Supporting Information is available free of charge at https://pubs.acs.org/doi/10.1021/acsnano.1c07693.

> Additional tables of coal properties; Raman analysis of laser-annealed/doped coals, graphene oxide, and graphene to explain the mechanism; XRD, sheet resistance analysis of laser-annealed coal thin films with different metal salts; magnetic hysteresis loops of coal-Co_3O_4 and coal-Fe_3O_4 particles at room temperature, 300 K (PDF)

AUTHOR INFORMATION

Corresponding Author

Xining Zang − *Department of Mechanical Engineering, Tsinghua University, Beijing 100084, China; Key Laboratory for Advanced Materials Processing Technology, Ministry of Education and State Key Laboratory of Tribology, Tsinghua University, Beijing 100084, China;* ⓞ orcid.org/0000-0001-6930-8060; Email: xzang@tsinghua.edu.cn

Authors

Nicola Ferralis − *Department of Materials Science and Engineering, Massachusetts Institute of Technology, Cambridge, Massachusetts 02139, United States*

Jeffrey C. Grossman − *Department of Materials Science and Engineering, Massachusetts Institute of Technology, Cambridge, Massachusetts 02139, United States;* ⓞ orcid.org/0000-0003-1281-2359

Complete contact information is available at:

https://pubs.acs.org/10.1021/acsnano.1c07693

Author Contributions

The manuscript was written through contributions of all authors. All authors have given approval to the final version of the manuscript. X.Z. designed and performed the experiments; N.F. provided insight on the coal chemistry; X.Z., N.F., and J.C.G. wrote the paper.

Notes

The authors declare no competing financial interest.

REFERENCES

(1) Park, S.; Kim, M.; Lim, Y.; Yu, J.; Chen, S.; Woo, S. W.; Yoon, S.; Bae, S.; Kim, H. S. Characterization of Rare Earth Elements Present in Coal Ash by Sequential Extraction. *J. Hazard. Mater.* **2021**, *402*, 123760.

(2) Taggart, R. K.; Hower, J. C.; Dwyer, G. S.; Hsu-Kim, H. Trends in the Rare Earth Element Content of U.S.-Based Coal Combustion Fly Ashes. *Environ. Sci. Technol.* **2016**, *50* (11), 5919−5926.

(3) Singer, L. S. Carbon Fibres from Mesophase Pitch. *Fuel* **1981**, *60* (9), 839−847.

(4) Jian, C.; Adams, J. J.; Grossman, J. C.; Ferralis, N. Carbon Fiber Synthesis from Pitch: Insights from ReaxFF Based Molecular Dynamics Simulations. *Carbon N. Y.* **2021**, *176*, 569.

(5) Zabihi, O.; Shafei, S.; Fakhrhoseini, S. M.; Ahmadi, M.; Naebe, M. Low-Cost Carbon Fibre Derived from Sustainable Coal Tar Pitch and Polyacrylonitrile : Fabrication. *Materials* **2019**, *12*, 1281.

(6) Yang, J.; Nakabayashi, K.; Miyawaki, J.; Yoon, S. Preparation of Pitch Based Carbon Fi Bers Using Hyper-Coal as a Raw Material. *Carbon N. Y.* **2016**, *106*, 28−36.

(7) Jiang, X.; Zhang, L.; Wang, F.; Liu, Y.; Guo, Q.; Wang, C. Investigation of Carbon Black Production from Coal Tar via Chemical Looping Pyrolysis. *Energy Fuels* **2016**, *30* (4), 3535−3540.

(8) Zhang, S.; Liu, Q.; Zhang, H.; Ma, R.; Li, K.; Wu, Y.; Teppen, B. J. Structural Order Evaluation and Structural Evolution of Coal Derived Natural Graphite during Graphitization. *Carbon N. Y.* **2020**, *157*, 714−723.

(9) Andrews, R.; Duddy, J.; Gellici, J.; Johnson, K.; Meyers, L.; Skoptsov, G.; Gellici, J.; Sarkus, T.; Giove, J. *Carbon Forward: Advanced Markets for Value-Added Products from Coal*; National Coal Council, 2021.

(10) Ali, S.; Atkins, R.; Bajura, R.; Collins, D.; Denton, D.; Duddy, J.; Eller, R.; Fischer, J.; Glesmann, S.; Gray, D.; Irwin, M.; James, D.; Johnson, K.; Jones, M.; Lovell, H.; Merle, G.; Oliver, J.; Palmer, F.; Roling, D.; Schultes, J.; Sjostrom, S.; Slone, D.; Judd, S. *Coal in a New Carbon Age Powering a Wave of Innovation in Advanced Products & Manufacturing*; National Coal Council, 2019.

(11) Kang, S.; Kim, K. M.; jung, K.; Son, Y.; Mhin, S.; Ryu, J. H.; Shim, K. B.; Lee, B.; Han, H. S.; Song, T. Graphene Oxide Quantum Dots Derived from Coal for Bioimaging: Facile and Green Approach. *Sci. Rep.* **2019**, *9* (1), 1−7.

(12) Ye, R.; Xiang, C.; Lin, J.; Peng, Z.; Huang, K.; Yan, Z.; Cook, N. P.; Samuel, E. L. G.; Hwang, C.-C.; Ruan, G.; Ceriotti, G.; Raji, A.-R. O.; Martí, A. A.; Tour, J. M. Coal as an Abundant Source of Graphene Quantum Dots. *Nat. Commun.* **2013**, *4* (1), 2943.

(13) Wang, Z.; Zhao, Z.; Qiu, J. Synthesis of Branched Carbon Nanotubes from Coal. *Carbon N. Y.* **2006**, *44* (7), 1321−1324.

(14) Jean, J.; Brown, P. R.; Jaffe, R. L.; Buonassisi, T.; Bulović, V. Pathways for Solar Photovoltaics. *Energy Environ. Sci.* **2015**, *8* (4), 1200−1219.

(15) Zhang, C.; Xie, Y.; Zhang, C.; Lin, J. Upgrading Coal to Multifunctional Graphene Based Materials by Direct Laser Scribing. *Carbon N. Y.* **2019**, *153*, 585−591.

(16) Zang, X.; Jian, C.; Ingersoll, S.; Li, H.; Adams, J. J.; Lu, Z.; Ferralis, N.; Grossman, J. C. Laser-Engineered Heavy Hydrocarbons: Old Materials with New Opportunities. *Sci. Adv.* **2020**, *6* (17), No. eaaz5231.

(17) Zang, X.; Tai, K. Y.; Jian, C.; Shou, W.; Matusik, W.; Ferralis, N.; Grossman, J. C. Laser-Induced Tar-Mediated Sintering of Metals and Refractory Carbides in Air. *ACS Nano* **2020**, *14* (8), 10413−10420.

(18) Keller, B. D.; Ferralis, N.; Grossman, J. C. Rethinking Coal: Thin Films of Solution Processed Natural Carbon Nanoparticles for Electronic Devices. *Nano Lett.* **2016**, *16* (5), 2951−2957.

(19) ASTM. *Standard Classification of Coals by Rank*; Annu. B. ASTM Stand. Vol 05.06; 2002.

(20) Zang, X.; Jian, C.; Zhu, T.; Fan, Z.; Wang, W.; Wei, M.; Li, B.; Follmar Diaz, M.; Ashby, P.; Lu, Z.; Chu, Y.; Wang, Z.; Ding, X.; Xie, Y.; Chen, J.; Hohman, J. N.; Sanghadasa, M.; Grossman, J. C.; Lin, L. Laser-Sculptured Ultrathin Transition Metal Carbide Layers for Energy Storage and Energy Harvesting Applications. *Nat. Commun.* **2019**, *10* (1), 3112.

(21) PARR, S. W. The Classification of Coal. *J. Ind. Eng. Chem.* **1922**, *14* (10), 919−922.

(22) Zhao, Y.; Liu, S.; Elsworth, D.; Jiang, Y.; Zhu, J. Pore Structure Characterization of Coal by Synchrotron Small-Angle X-Ray Scattering and Transmission Electron Microscopy. *Energy Fuels* **2014**, *28* (6), 3704−3711.

(23) Jin, Z.; Zhang, Z.; Demir, K.; Gu, G. X. Machine Learning for Advanced Additive Manufacturing. *Matter* **2020**, *3* (5), 1541−1556.

(24) Lin, J.; Peng, Z.; Liu, Y.; Ruiz-Zepeda, F.; Ye, R.; Samuel, E. L. G.; Yacaman, M. J.; Yakobson, B. I.; Tour, J. M. Laser-Induced Porous Graphene Films from Commercial Polymers. *Nat. Commun.* **2014**, *5*, 5−12.

(25) Ye, R.; Chyan, Y.; Zhang, J.; Li, Y.; Han, X.; Kittrell, C.; Tour, J. M. Laser-Induced Graphene Formation on Wood. *Adv. Mater.* **2017**, *29* (37), 1−7.

(26) Morris, O. P.; Zang, X.; Gregg, A.; Keller, B.; Getachew, B.; Ingersoll, S.; Elsen, H. A.; Disko, M. M.; Ferralis, N.; Grossman, J. C. Natural Carbon By-Products for Transparent Heaters: The Case of Steam-Cracker Tar. *Adv. Mater.* **2019**, *31* (35), 1900331.

(27) Zang, X.; Shen, C.; Chu, Y.; Li, B.; Wei, M.; Zhong, J.; Sanghadasa, M.; Lin, L. Laser-Induced Molybdenum Carbide-Graphene Composites for 3D Foldable Paper Electronics. *Adv. Mater.* **2018**, *30* (26), 1800062.

(28) Ferrari, A. C. Raman Spectroscopy of Graphene and Graphite: Disorder, Electron-Phonon Coupling, Doping and Nonadiabatic Effects. *Solid State Commun.* **2007**, *143* (1−2), 47−57.

(29) Burnham, A. K. *Global Chemical Kinetics of Fossil Fuels*; Springer International Publishing, 2017, DOI: 10.1007/978-3-319-49634-4.

(30) Liu, Y.; Ferralis, N.; Bryndzia, L. T.; Grossman, J. C. Genome-Inspired Molecular Identification in Organic Matter via Raman Spectroscopy. *Carbon N. Y.* **2016**, *101*, 361−367.

(31) Ferralis, N.; Matys, E. D.; Knoll, A. H.; Hallmann, C.; Summons, R. E. Rapid, Direct and Non-Destructive Assessment of Fossil Organic Matter via MicroRaman Spectroscopy. *Carbon N. Y.* **2016**, *108*, 440−449.

(32) Ferralis, N.; Liu, Y.; Bake, K. D.; Pomerantz, A. E.; Grossman, J. C. Direct Correlation between Aromatization of Carbon-Rich Organic Matter and Its Visible Electronic Absorption Edge. *Carbon N. Y.* **2015**, *88*, 139−147.

(33) Cheng, W.; Xue, J.; Xie, J.; Zhou, G.; Nie, W. A Model of Lignite Macromolecular Structures and Its Effect on the Wettability of Coal: A Case Study. *Energy Fuels* **2017**, *31* (12), 13834−13841.

(34) Zang, X.; Shen, C.; Chu, Y.; Li, B.; Wei, M.; Zhong, J.; Sanghadasa, M.; Lin, L. Laser-Induced Molybdenum Carbide-

(35) Ferrari, A. C.; Robertson, J. Interpretation of Raman Spectra of Disordered and Amorphous Carbon. *Phys. Rev. B* **2000**, *61* (20), 14095−14107.

(36) Jian, C.; Merchant, S.; Zang, X.; Ferralis, N.; Grossman, J. C. Structural Evolutions of Small Aromatic Mixtures under Extreme Temperature Conditions: Insights from ReaxFF Molecular Dynamics Investigations. *Carbon N. Y.* **2019**, *155*, 309−319.

(37) Wang, X.; Li, X.; Zhang, L.; Yoon, Y.; Weber, P. K.; Wang, H.; Guo, J.; Dai, H. N-Doping of Graphene Through Electrothermal Reactions with Ammonia. *Science (80-.).* **2009**, *324* (5928), 768−771.

(38) Zhao, L.; He, R.; Rim, K. T.; Schiros, T.; Kim, K. S.; Zhou, H.; Gutierrez, C.; Chockalingam, S. P.; Arguello, C. J.; Palova, L.; Nordlund, D.; Hybertsen, M. S.; Reichman, D. R.; Heinz, T. F.; Kim, P.; Pinczuk, A.; Flynn, G. W.; Pasupathy, A. N. Visualizing Individual Nitrogen Dopants in Monolayer Graphene. *Science (80-.).* **2011**, *333* (6045), 999−1003.

(39) Zhang, C.; Fu, L.; Liu, N.; Liu, M.; Wang, Y.; Liu, Z. Synthesis of Nitrogen-Doped Graphene Using Embedded Carbon and Nitrogen Sources. *Adv. Mater.* **2011**, *23* (8), 1020−1024.

(40) Błoński, P.; Tuček, J.; Sofer, Z.; Mazánek, V.; Petr, M.; Pumera, M.; Otyepka, M.; Zbořil, R. Doping with Graphitic Nitrogen Triggers Ferromagnetism in Graphene. *J. Am. Chem. Soc.* **2017**, *139* (8), 3171−3180.

(41) Lin, L.; Li, J.; Yuan, Q.; Li, Q.; Zhang, J.; Sun, L.; Rui, D.; Chen, Z.; Jia, K.; Wang, M.; Zhang, Y.; Rummeli, M. H.; Kang, N.; Xu, H. Q.; Ding, F.; Peng, H.; Liu, Z. Nitrogen Cluster Doping for High-Mobility/Conductivity Graphene Films with Millimeter-Sized Domains. *Sci. Adv.* **2019**, *5* (8), No. eaaw8337.

(42) Zhang, L. L.; Zhao, X.; Ji, H.; Stoller, M. D.; Lai, L.; Murali, S.; McDonnell, S.; Cleveger, B.; Wallace, R. M.; Ruoff, R. S. Nitrogen Doping of Graphene and Its Effect on Quantum Capacitance, and a New Insight on the Enhanced Capacitance of N-Doped Carbon. *Energy Environ. Sci.* **2012**, *5* (11), 9618−9625.

(43) Calabro, R. L.; Yang, D. S.; Kim, D. Y. Controlled Nitrogen Doping of Graphene Quantum Dots through Laser Ablation in Aqueous Solutions for Photoluminescence and Electrocatalytic Applications. *ACS Appl. Nano Mater.* **2019**, *2* (11), 6948−6959.

(44) Li, H.; Zhu, T.; Ferralis, N.; Grossman, J. C. Charge Transport in Highly Heterogeneous Natural Carbonaceous Materials. *Adv. Funct. Mater.* **2019**, *29* (38), 1904283.

(45) Wakeland, S.; Martinez, R.; Grey, J. K.; Luhrs, C. C. Production of Graphene from Graphite Oxide Using Urea as Expansion-Reduction Agent. *Carbon N. Y.* **2010**, *48* (12), 3463−3470.

(46) Chamoli, P.; Das, M. K.; Kar, K. K. Urea-Assisted Low Temperature Green Synthesis of Graphene Nanosheets for Transparent Conducting Fi Lm. *J. Phys. Chem. Solids* **2018**, *113*, 17−25.

(47) DeMeo, D.; MacNaughton, S.; Sonkusale, S.; Vandervelde, T. Electrodeposited Copper Oxide and Zinc Oxide Core-Shell Nanowire Photovoltaic Cells. In *Nanowires - Implementations and Applications*; InTech, 2011.

(48) Shen, Y. F.; Tang, J.; Nie, Z. H.; Wang, Y. D.; Ren, Y.; Zuo, L. Preparation and Application of Magnetic Fe3O4 Nanoparticles for Wastewater Purification. *Sep. Purif. Technol.* **2009**, *68* (3), 312−319.

(49) Manoharan, H. C.; Lutz, C. P.; Eigler, D. M. Quantum Mirages Formed by Coherent Projection of Electronic Structure. *Nature* **2000**, *403* (6769), 512−515.

(50) Mohapatra, J.; Zeng, F.; Elkins, K.; Xing, M.; Ghimire, M.; Yoon, S.; Mishra, S. R.; Liu, J. P. Size-Dependent Magnetic and Inductive Heating Properties of Fe3O4 Nanoparticles: Scaling Laws across the Superparamagnetic Size. *Phys. Chem. Chem. Phys.* **2018**, *20*, 12879.

(51) Mao, G.; Drack, M.; Karami-Mosammam, M.; Wirthl, D.; Stockinger, T.; Schwödiauer, R.; Kaltenbrunner, M. Soft Electromagnetic Actuators. *Sci. Adv.* **2020**, *6* (26), DOI: 10.1126/sciadv.abc0251.

H

(52) Purtova, T.; Schumacher, H. Overview of RF MEMS Technology and Applications. In *Handbook of Mems for Wireless and Mobile Applications*; Elsevier, 2013; pp 3−29.

(53) Speight, J. G. *The Chemistry and Technology of Coal*, 3rd ed.; CRC Press, 2012.

(54) Library Guides: Pennsylvania Mines and Mining: General Information https://guides.libraries.psu.edu/PAMinesandMining%0A.

(55) Lei, Z.; Lu, L.; Zhao, X. S. The Electrocapacitive Properties of Graphene Oxide Reduced by Urea. *Energy Environ. Sci.* **2012**, *5*, 6391.